# Synthesis, crystal structure, and vibrational studies of the monoclinically distorted double perovskite, $Sr_2Mn_{1-x}Ni_xTeO_6$ with ($x = 0.25$, 0.5, and 0.75)

A. Zaraq,[1,a] B. Orayech,[2] J. M. Igartua,[3] and A. El Bouari[1]
[1]*Laboratoire de Physico-Chimie des Matériaux Appliqués (LPCMA), Université Hassan II de Casablanca, Faculté des Sciences Ben M'sik, Avenue Idriss El harti, B.P. 7955, Casablanca, Morocco*
[2]*Maxam, Technology Center Energetic Materials, Carretera N-623 km 28. 09141 Quintanilla Sobresierra. Burgos, Spain*
[3]*Fisika Aplikatua II Saila, Zientzia eta Teknologia Fakultatea, Euskal Herriko Unibertsitatea, P.O.Box 644, Bilbao 48080, Spain*

(Received 27 August 2018; accepted 13 April 2019)

The new double perovskite oxides $Sr_2Mn_{1-x}Ni_xTeO_6$ with $x = 0.25$, 0.5 and 0.75 have been synthesized in polycrystalline form by a conventional solid-state reactions process at 1180 °C, in the air. The structural and vibrational properties of these materials were studied by means XRPD, Raman, and IR spectroscopy. It has been proven that all the materials show typical double perovskite structures with a monoclinic symmetry, but with two different space group, $P2_1/n$ for the compositions ($x = 0.25$ and 0.5), while the composition ($x = 0.75$) crystallizes in the space group $I2/m$. The lattice parameters obtained are in agreement with those of the two pure extremes $Sr_2MnTeO_6$ and $Sr_2NiTeO_6$. The monoclinic structural distortion involves long range ordering between $Te^{6+}$ (in 2*b* site) and a random mixture ($Mn^{2+}/Ni^{2+}$) (in 2*a* site) for the two compositions ($x = 0.25$ and 0.5) that crystallize in $P2_1/n$. For the material ($x = 0.75$) with $I2/m$, similar distortion, ordering and mixing occur at the *B* and *B*' double perovskite sites. It was observed that Vegard Law is satisfied, taking into account the cell parameters of both extremes. The effect of the partial substitution of Mn by Ni was also seen in Raman and IR data where a significant mode shift was observed with nickel content increase.
 [doi:10.1017/S0885715619000411]

Key words: $Sr_2Mn_{1-x}Ni_xTeO_6$ double perovskites oxides, X-ray diffraction, Rietveld refinements, Raman spectroscopy, infrared spectroscopy, crystal structure

## I. INTRODUCTION

Over the last few decades, the double-perovskite structure compounds with the general formula $A_2BB'O_6$ (*A* = alkaline, alkaline-earth, or rare-earth ions, *B* and *B*' = transition metal ions) have been studied extensively for their potential applications in ferroelectrics, catalysis, magnetic media, and microwave dielectrics (Gandhi and Keshri, 2015; Tasca *et al*., 2017; Halder *et al*., 2018; Li *et al*., 2018). Depending on their valences and relative radii, the *B* (*B*') sites can be occupied by two different transition metal ions; therefore, a broad range of chemical and physical properties may be expected in this system (Zamkova *et al*., 2013). The double perovskite oxides structures $A_2BB'O_6$ can be reported as a modification of the simple structure $ABO_3$ with the *B* positions occupying by the association of $BO_6$ and $B'O_6$ octahedral of acceptable charge and size. If *B* and *B*' are satisfactorily different the ordered double perovskite structure is produced. However, the combinations of lattice distortions and orderings of different types of *B* (*B*') cations lead to the reduction of symmetry from the ideal cubic structure $Fm\bar{3}m$, and even small changes produced in the tilting of the $B/B'O_6$ octahedral can lead to either a tetragonal or a monoclinic distortion in these materials (Pena and Fierro, 2001; Knapp and Woodward, 2006; Ochi *et al*., 2013). The distortions of double perovskite, sometimes very subtle, are often the cause of the important physical, electronic, and magnetic properties of them (Mugavero *et al*., 2005; Bernardo *et al*., 2014; Ghimire *et al*., 2016).

The materials of double perovskite structure are known by a phase transition behavior under the effect of isomorphic substitutions in sites *A* and *B* of the double perovskite structure, temperature and/or pressure (Han *et al*., 2013; Orayech *et al*., 2015; Zaraq *et al*., 2016).

Many studies have been done on double perovskites with hexavalent cations, such as Sb, Nb, Mo, Re, W, Ta, and Te (Cecilia Blanco *et al*., 2014; Musa Saad 2014). As reported by (Tang *et al*., 2016, 2017) the *p*-block elements such as tellurium can be strongly stabilized in the *B*-sites of the perovskite structure, presenting the required spherical symmetry and adequate ion size. From the 1940s, $Sr_2NiTeO_6$ oxide has been a great importance in the scientific community. The first studies focused on its properties, such as dielectric material for capacitors (Venevtsev *et al*., 1974). The symmetry of the crystal of $Sr_2NiTeO_6$ is $I2/m$ and its cell parameters are: $a = 7.9174(4)$ Å, $b = 7.8765(4)$ Å, $c = 7.916(1)$ Å, and $\beta = 90.378°$ (Ortega-San Martin *et al*., 2005a, 2005b). Concerning the oxides, $Sr_2MnTeO_6$ have shown that this material has a monoclinic structure with $P2_1/n$ space group (Ortega-San Martin *et al*., 2004).

In this work, we present a complete analysis by XRPD, Raman, and infrared (IF) spectroscopy of double perovskite oxides $Sr_2Mn_{1-x}Ni_xTeO_6$ (with $x = 0.25$, 0.5, and 0.75). The change in this series with the composition (*x*) is proposed for the first time. Furthermore, the structural phase

[a]Author to whom correspondence should be addressed. Electronic mail: assmaa.zaraq@gmail.com

transition at room temperature and with the nickel change is also analyzed.

## II. EXPERIMENTAL

### A. Sample preparation

The polycrystalline phases of the compositions $Sr_2Mn_{1-x}Ni_xTeO_6$ with ($x = 0.25$, 0.5, and 0.75) were synthesized by conventional high-temperature solid-state reaction from stoichiometric amounts of $TeO_2$ (99.9%), Mn $(NO_3)_2.4H_2O$ (99.999%), and $Ni(NO_3)_2.6H_2O$ (99.9%) with the appropriate metal carbonate of $SrCO_3$ (99.9%). All compounds used as received from Sigma-Aldrich. The samples were heated in air, in alumina crucibles, at progressively higher temperatures (300 °C/6 h, 600 °C/12 h, 800 °C/12 h, 900 °C/24 h, 1000 °C/24 h, and 1180 °C/24 h) with periodic intermediate grinding.

The chemical reaction is:

$$2SrCO_3 + (1-x)Mn(NO_3)_2.4H_2O + xNi(NO_3)_2.6H_2O + TeO_2 \rightarrow Sr_2Mn_{1-x}Ni_xTeO_6 + 2CO_2\uparrow + (1+2x)H_2O\uparrow + 2NH_3\uparrow + 5/2O_2\uparrow (x = 0.25,\ 0.5,\ \text{and}\ 0.75)$$

### B. XRPD measurements

The final products of chemistry reactions were characterized by X-ray powder diffraction (XRPD) at room temperature with an Analytical X'Pert-PRO ($\theta-2\theta$) diffractometer, using Cu$K\alpha$ radiation (45 kV, 40 mA). The data were collected from 13 to 80° $2\theta$, through steps of 0.01 ($2\theta$). The refinements of the structures were achieved by the Rietveld method employing the FullProf program (Rodriguez-Carvajal, 1997; Roisnel and Rodriquez-Carvajal, 2001). The peaks of the XRPD lines were defined using a pseudo-Voigt function, concerning the background, is adapted with a fifth order polynomial. The structural refinement by the Rietveld method of the observed XXRPD data is begun with scale and the others parameters are refined according to this order: scale factor, zero shift, the cell parameters, background, atomic positions, asymmetry parameters, and the parameters of thermal motion of the atoms.

### C. Raman and infrared spectroscopy

The Raman spectra were reported on DXR2 Raman Microscope. The spectral range is 3500–100 $cm^{-1}$ captured with a single exposure of the CCD for avoids stitching artifacts, a laser type diode pumped, solid state (DPSS) (Spectra-Physics, 600 nm, 8 mW), and an optical system (with spectral resolution 2 $cm^{-1}$ FWHM). All measurements were carried out at room temperature.

The IF spectra were recorded in the form of KBr pellets in the wave number range 4000–400 $cm^{-1}$ using a Mattson 7000 spectrometer, then they are treated using the Win-IR software.

## III. RESULTS AND DISCUSSION

### A. Indexing and refinement of structures by the Rietveld method

The XRPD patterns of $Sr_2Mn_{1-x}Ni_xTeO_6$ ($x = 0.25$, 0.5, and 0.75) represented in Figure 1, indicated that the peak positions of the XRPD lines are analogous to those observed in the literature of the other double perovskite-type (e.g., $Sr_2CoTeO_6$; $Sr_2CaTeO_6$...) (Prior *et al.*, 2005; Ortega-San Martin *et al.*, 2005a, 2005b). The double perovskite formula $Sr_2Mn_{1-x}Ni_xTeO_6$ is isostructural with double perovskite-type phases $Sr_2MnTeO_6$ and $Sr_2NiTeO_6$ crystallizing in the space groups $P2_1/n$ and $I2/m$, respectively (Ortega-San Martin *et al.*, 2004; Ortega-San Martin *et al.*, 2005a, 2005b).

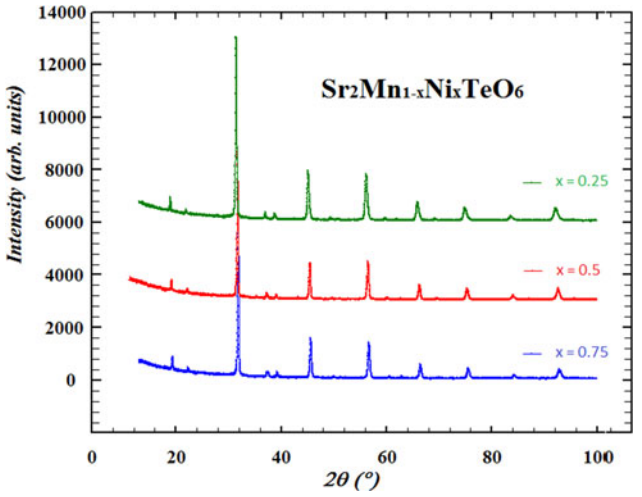


Figure 1. (Colour online) X-ray powder diffraction patterns for $Sr_2Mn_{1-x}Ni_xTeO_6$ ($x = 0.25$, 0.5, and 0.75).

The tolerance factors, $t$, at room temperature of the titled series, have been calculated using the ionic radius suggested in Shannon database (Shannon, 1976) and the obtained values are listed in Table I. The values of tolerance factor suggest, in the one hand, that the room-temperature structures of both compounds should not be cubic, and, in the other hand, that $Sr_2Mn_{0.75}Ni_{0.25}TeO_6$ and $Sr_2Mn_{0.5}Ni_{0.5}TeO_6$ compounds will be more distorted than $Sr_2Mn_{0.25}Ni_{0.75}TeO_6$.

For a structural study of this double perovskite series $Sr_2Mn_{1-x}Ni_xTeO_6$, we had to choose between the two space groups ($P2_1/n$ and $I2/m$). And of course, Miller's index always comes down to minimizing the number of space groups to be considered in the structural study, for that, two $2\theta$ regions were analysis. The first region of (24–26°) corresponds to the reflections [($\bar{1}$ 11) (111)] and the second region of (52–53°) concerns the reflections [(−311) (311), (131) (−131)], these reflections characterize the primitive peaks $h + k + 1 = 2n + 1$ of the usual $P2_1/n$ ($a^-a^-c^+$) space group.

Moreover, in Figure 2, we have observed the presence of the characteristic systematic reflections [($\bar{1}$ 11) (111)] and [(−311) (311) (131) (−131)] in the X-ray diffraction pattern of the two compositions ($x = 0.25$ and 0.5), while these reflections disappeared from the X-ray diffraction pattern of the composition ($x = 0.75$).

TABLE I. Tolerance factor calculated using the ionic radii suggested in (Shannon, 1976).

| Compound | Tolerance factor |
|---|---|
| $Sr_2MnTeO_6$ | 0.9561 |
| $Sr_2Mn_{0.75}Ni_{0.25}TeO_6$ | 0.9641 |
| $Sr_2Mn_{0.5}Ni_{0.5}TeO_6$ | 0.9722 |
| $Sr_2Mn_{0.25}Ni_{0.75}TeO_6$ | 0.9805 |
| $Sr_2NiTeO_6$ | 0.9881 |


https://doi.org/10.1017/S0885715619000411 Published online by Cambridge University Press

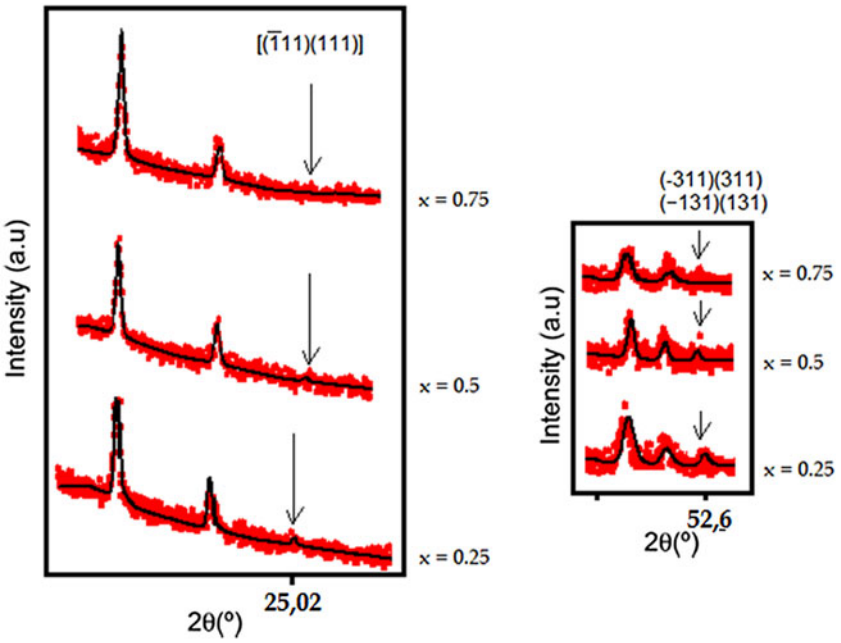


Figure 2. (Colour online) Selected $2\theta$ intervals for the three compositions of the $Sr_2Mn_{1-x}Ni_xTeO_6$ series ($x$ = 0.25, 0.5, and 0.75) determined the reflections characterizing the primitive peaks of the usual $P2_1/n$ space group with $h+k+1=2n+1$. (a) The reflections [($\bar{1}$11)(111)] located around 25.01 and 25.06°. (b) The reflections [(−311)(311), (−131)(131)] located around 52.57 and 52.90°.

Via the method of Rietveld and using a FullProf analysis program the crystal structures of the compositions $Sr_2Mn_{1-x}Ni_xTeO_6$ ($x$ = 0.25, 0.5, and 0.75) were tested. We have done the structural refinement with both models of symmetry $P2_1/n$ and $I2/m$ for all the series. We noticed good values of reliability factors for the compositions ($x$ = 0.25 and 0.5) with the symmetry space group $P2_1/n$ (International Tables, No. 14) (Glazer notation $a^+a^-a^-$) (Glazer, 1975). While for the composition ($x$ = 0.75) the refinement with the symmetry $P2_1/n$ leads to relatively larger values of reliability factors (e.g., $R_B$ = 8.6%).

But when we have done the structural refinement with $I2/m$ symmetry (International Tables, No. 12), (Glazer notation $a^0b^-b^-$) (Glazer, 1975) of the formula with ($x$ = 0.75), surprisingly, this refinement led to acceptable reliability factors (e.g., $R_B$ = 4.24%). The details of Rietveld refinement conditions of this series are recorded in Table II.

The variation at room temperature of the lattice parameters and the unit cell volume as a function of the tolerance factor, of the series $Sr_2Mn_{1-x}Ni_xTeO_6$ is shown in Figure 3. As can be seen from Figure 3(a) there is a gradual decrease in the cell parameters when the nickel amount increases, and that owing to the lower ionic radius of $Ni^{2+}$ (0.69 Å) compared to $Mn^{2+}$ (0.83 Å). This difference between the size of $Ni^{2+}$ and $Mn^{2+}$ is responsible for the monoclinic distortion between the compositions of this double perovskite series. The decreasing of the volume of the $BO_6$ octahedral leads to the decrease in the tilt systems which is observed by decreasing the

TABLE II. Refined parameters for $Sr_2Mn_{1-x}Ni_xTeO_6$ at room temperature from XRPD data.

| Compositions | $x$ = 0 | $x$ = 0.25 (PW) | $x$ = 0.5 (PW) | $x$ = 0.75 (PW) | $x$ = 1 |
|---|---|---|---|---|---|
| Wavelength (Å) | $k\alpha1$ = 1.54056 | $k\alpha1$ = 1.54056 | $k\alpha1$ = 1.54056 | $k\alpha1$ = 1.54056 | $k\alpha1$ = 1.54056 |
| $2\theta$ step scan increment (°) | 0.010 | 0.010 | 0.010 | 0.010 | 0.010 |
| $2\theta$ range (°) | 10–100 | 10–100 | 10–100 | 10–100 | 10–100 |
| Program | FullProf | FullProf | FullProf | FullProf | FullProf |
| Zero point ($2\theta$°) | −0.23773 | −0.23793 | −0.03383 | 0.05022 | −0.02843 |
| Pseudo-Voigt function | | | | | 0.30897 |
| PV = $\eta$ L + (1 − $\eta$) G | 0.50628 | 0.46154 | 0.55141 | 0.58645 | |
| No. of refined parameters | 31 | 29 | 30 | 63 | 15 |
| Crystal system | Monoclinic | Monoclinic | Monoclinic | Monoclinic | Monoclinic |
| Space group | $P2_1/n$ | $P2_1/n$ | $P2_1/n$ | $I2/m$ | $I2/m$ |
| $a$ (Å) | 5.7009(1) | 5.6542(1) | 5.6476(1) | 5.6285(1) | 5.6166(1) |
| $b$ (Å) | 5.6770 (1) | 5.6172(1) | 5.6290(1) | 5.6250(1) | 5.5807(1) |
| $c$ (Å) | 8.0334 (1) | 7.9979(1) | 7.9514(1) | 7.9430(1) | 7.8797(1) |
| $\beta$ (°) | 90.085 (1) | 90.089(2) | 90.047(2) | 90.030(2) | 90.048(2) |
| $V$ (Å3) | 259.994(10) | 254.023(10) | 252.781(10) | 251.953(10) | 246.97(10) |
| $Z$ | 2 | 2 | 2 | 2 | 2 |
| Atom number | 4 | 10 | 10 | 9 | 4 |
| $R_p$ | 8.0 | 7.43 | 6.97 | 7.09 | 9.2 |
| $R_{wp}$ | 14.7 | 10.2 | 9.40 | 9.43 | 13.1 |
| $R_{exp}$ | 5.1 | 7.06 | 7.96 | 7.71 | 5.2 |
| $R_B$ | 2.40 | 6.30 | 5.40 | 4.24 | 4.00 |
| $R_F$ | 4.20 | 5.90 | 5.95 | 3.56 | 5.00 |
| $\chi^2$ | 2.10 | 2.09 | 1.39 | 1.50 | 2.1 |

(PW), Present work.


https://doi.org/10.1017/S0885715619000411 Published online by Cambridge University Press

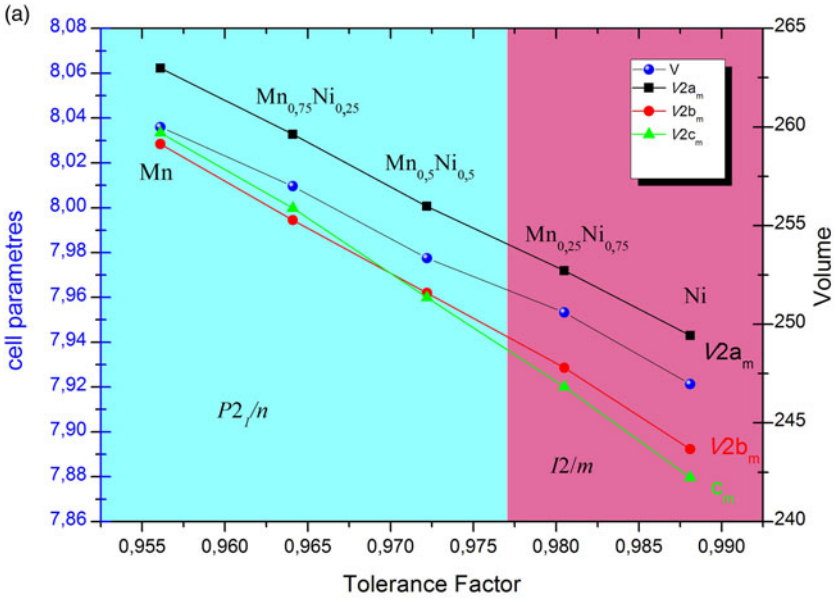


Figure 3. (Colour online) Variations of (a) the cell parameters and (b) $\beta$ angle as a function of the tolerance factor for $Sr_2Mn_{1-x}Ni_xTeO_6$ ($x = 0.25$, 0.5, and 0.75).

monoclinic angle [see Figure 3(b)]. Therefore, when the size of the cations in site *B* is small, the tilt of the octahedron is weak and the structure is symmetrical.

As indicated in several reports, in materials of double perovskite structure and holding rare earth ions, the kind and the size of the elements seems to be the reason of selective occupancy of their sites *B* and *B*' (Azad *et al.*, 2004). As many articles demonstrate that both *B* and *B*' sites, in the double perovskite formula $A_2BB'O_6$, are able to be occupied either by manganese and/or nickel and also tellurium atoms as it was noticed, for example, in $Sr_2MnTeO_6$ (Ortega-San Martin *et al.*, 2004) and $Sr_2NiTeO_6$ (Ortega-San Martin *et al.*, 2005a, 2005b) [(Mn/Ni) $B_6$(Te)$B'O_6$]. It is quite common that $Te^{6+}$ ($r_{VI}$ $Te^{6+} = 0.56$ Å) ion favor to keep the octahedral *B*' site of $A_2BB'O_6$ double perovskite, and the $Ni^{2+}$ and $Mn^{2+}$ cations ($r_{II}$ $Ni^{2+} = 0.69$ Å, $r_{II}$ $Mn^{2+} = 0.83$ Å) prefer to be in site *B*, we recognize that there is a comparatively important difference between their ionic radii (Shannon, 1976). In order to clarify the cationic distribution in the double perovskite series $Sr_2Mn_{1-x}Ni_xTeO_6$, the structural refinement was based on two main assumptions.

In the first proposed Rietveld model, starting atomic positions for the Rietveld refinement of $Sr_2Mn_{0.75}Ni_{0.25}TeO_6$ and $Sr_2Mn_{0.5}Ni_{0.5}TeO_6$ were based on those reported for $Sr_2MnTeO_6$ ($P2_1/n$ space group) (Ortega-San Martin *et al.*, 2004). For $Sr_2Mn_{0.25}Ni_{0.75}TeO_6$ the beginning atomic positions were based on those mentioned for $Sr_2NiTeO_6$ ($I2/m$ space group) (Ortega-San Martin *et al.*, 2005a, 2005b). For the two compositions ($x = 0.25$ and 0.5) the Mn and Ni atoms were restricted to be in the 2*a* (0 0 0) positions (*B* site) and the Te atoms are assumed to be only in the 2*b* (0, 0, ½) positions (*B*' site). Concerning the material $Sr_2Mn_{0.25}Ni_{0.75}TeO_6$, the (Mn, Ni) and Te atoms are supposed to reside at the 2*d* (½, ½, 0) and 2*a* (0, 0, 0) positions, respectively. The occupancy factors for (Mn/Ni) and Te atoms within the two possible positions were not allowed to vary. This first refinement resulted in negative values for the displacement parameters (Biso) of Mn and Ni in (2*a* and 2*d*) sites, and big values of (Biso) for Te (2*b* and 2*a*) sites for the two symmetries $P2_1/n$ and $I2/m$. Actually, the negative values for the displacement parameters of Mn and Ni indicate an electronic deficit within the 2*a* site in $P2_1/n$ and the same thing happened into 2*d* site in the $I2/m$ space group. Concerning the highest values of (Biso) for Tellerium atoms reveal an overabundance of electronic density. Even though


https://doi.org/10.1017/S0885715619000411 Published online by Cambridge University Press

the results of this refinement are not too favorable, they clearly demonstrate the essentiality of assuming the distribution of a heavier atom than Ni and Mn in the *B* sites of the compounds $Sr_2Mn_{1-x}Ni_xTeO_6$. Absolutely, given that $Sr_2Mn_{1-x}Ni_xTeO_6$ contains Tellerium atoms, which have a comparatively high atomic number [*Z*(Te) = 52].

In the second proposed Rietveld model for the two materials $Sr_2Mn_{0.75}Ni_{0.25}TeO_6$ and $Sr_2Mn_{0.5}Ni_{0.5}TeO_6$, (Mn, Ni, and Te) atoms are distributed between the two 2*a* and 2*b* positions of the *B* and *B*' sites. The same thing about the compound $Sr_2Mn_{0.25}Ni_{0.75}TeO_6$, these atoms are distributed between 2*d* and 2*a* of the *B* and *B*' sites of the double perovskite structure. The contrast provided between ($Mn^{2+}$/$Ni^{2+}$) and $Te^{6+}$ allowed the free refinement of the occupancy factors of these atoms over the *B* and *B*' sites during refining X-ray diffraction data. This fact is to conserve the total cation contents to be the same as the stoichiometry as the initial synthesized mixture. If not, the model is not able to correctly reproduce the experimental intensity of many peaks in the pattern. The occupancy rates of the oxygen atom sites have not been refined because they can only be measured accurately by neutron diffraction. In particular, this structural refinement leads to acceptable values for the coefficients of thermal motion (Biso) for all the double perovskite series, in addition it gave very satisfactory factors of reliability.

The final obtained cationic distribution that satisfactorily reproduces all the characteristics of the pattern is [$Sr_2$ ($Mn_{0.623}Ni_{0.226}Te_{0.177}$)*B* ($Mn_{0.127}Ni_{0.024}Te_{0.823}$)*B*'$O_6$ for *x* = 0.25, $Sr_2$ ($Mn_{0.434}Ni_{0.366}Te_{0.166}$)*B* ($Mn_{0.066}Ni_{0.134}Te_{0.834}$) *B*'$O_6$ for *x* = 0.5, and $Sr_2$ ($Mn_{0.195}Ni_{0.605}Te_{0.155}$)*B* ($Mn_{0.055}$ $Ni_{0.145}Te_{0.845}$)*B*'$O_6$ for *x* = 0.75].

Concerning the $Sr^{2+}$ and [O(1), O(2), and O(3)] atoms were allowed at the 4*e* (*x*, *y*, *z*) and 4*e* (*x*, *y*, *z*) positions, respectively, for both compositions (*x* = 0.25 and 0.5). About the composition (*x* = 0.75) crystalizing in *I*2/*m* space group, the $Sr^{2+}$, O(1), and O(2) atoms occupy the 4*i* (*x*, 0, *z*), 4*i* (*x*, 0, *z*), and 8*j* (*x*, *y*, *z*) sites, respectively.

The experimental and calculated XRPD from the last proposed Rietveld model are compared in Figure 4, over the 2$\theta$ range from 17 to 100°, showing a good agreement between the profiles observed and calculated at ambient temperature. The refined position for the three phases is also displayed in Table III.

### B. Description of the structure

In Figure 5(a), the crystal structures show the connection between the octahedras $(Mn/Ni/Te)_{2a}O_6$ and $(Mn/Ni/Te)_{2b}O_6$ and Figure 5(c) shows the perovskite structure with $P2_1/n$ symmetry that is anticipated by the tilt system ($a^+a^-a^-$)

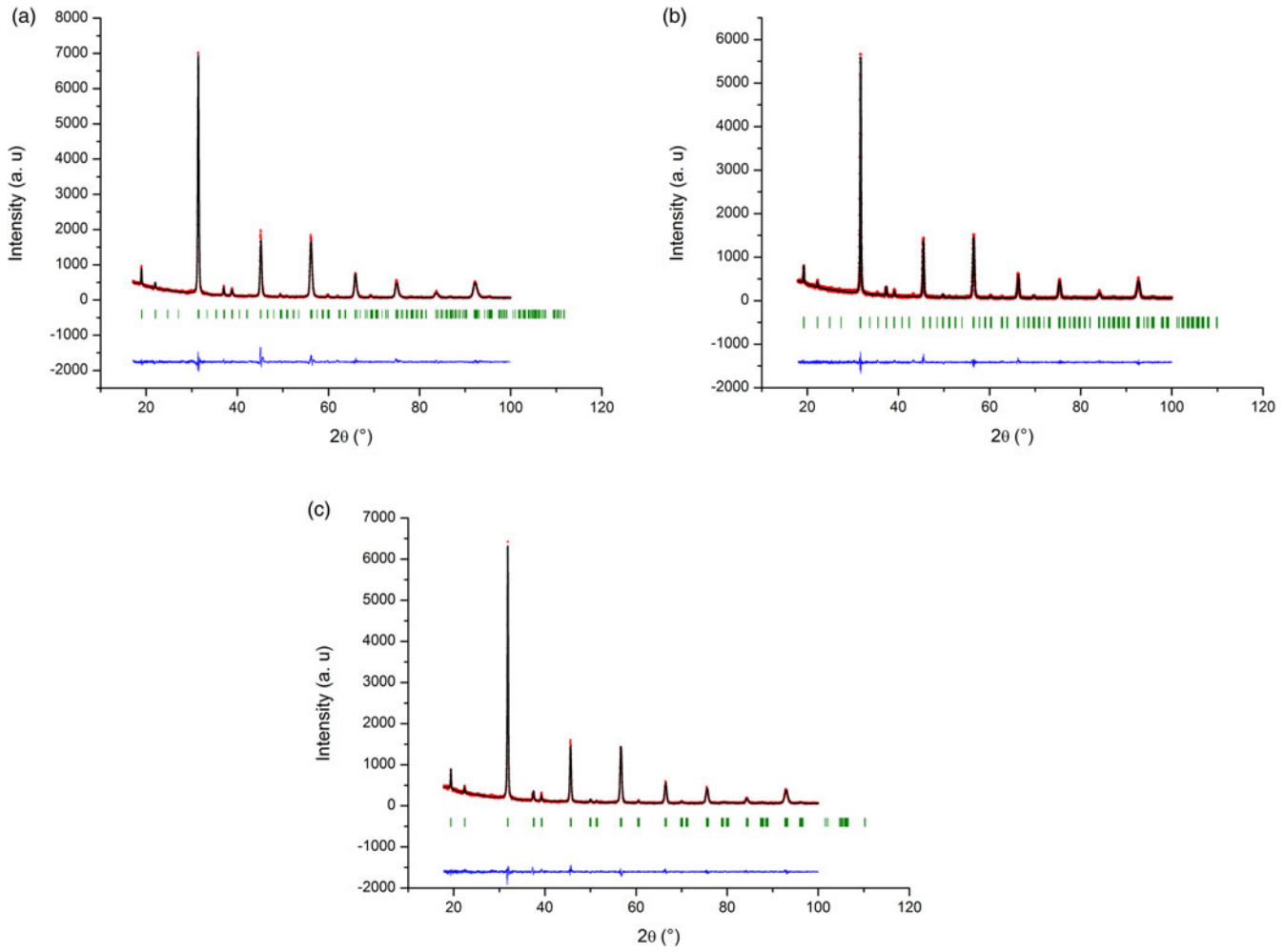


Figure 4. (Colour online) Experimental (symbols) and calculated (line) powder diffraction profiles for the Rietveld refinement of the series (a) $Sr_2Mn_{0.75}Ni_{0.25}TeO_6$, (b) $Sr_2Mn_{0.5}Ni_{0.5}TeO_6$ and (c) $Sr_2Mn_{0.25}Ni_{0.75}TeO_6$ at room temperature. The bars in the less part of the graphics symbolize the Bragg peak positions.


https://doi.org/10.1017/S0885715619000411 Published online by Cambridge University Press

TABLE III. Atomic position, displacement parameters, fractional coordinates and occupation parameters for the series $Sr_2Mn_{1-x}Ni_xTeO_6$ with ($x = 0.25$, 0.5, and 0.75) after Rietveld refinement from XRPD data collected at room temperature.

| Atom | Wyckoff site | $X$ | $y$ | $z$ | $B$(Å$^2$) | Occ. |
|---|---|---|---|---|---|---|
| $x = 0.25$ ($P2_1/n$) | | | | | | |
| Sr | 4*e* | 0.4860(14) | 0.0107(8) | 0.2602(9) | 1.57(5) | 2.0000 |
| Ni1/Mn1/Te1 | 2*a* | 0.0000 | 0.0000 | 0.0000 | 0.5(4) | 0.220(5)/0.620(5)/0.170(5) |
| Ni2/Mn2/Te2 | 2*b* | 0.0000 | 0.0000 | 0.5000 | 2.1(3) | 0.030(5)/0.13(5)/0.840(5) |
| O1 | 4*e* | 0.958(9) | −0.001(5) | 0.744(5) | 1.0000 | 2.0000 |
| O2 | 4*e* | 0.268(8) | 0.247(11) | 1.007(7) | 1.0000 | 2.0000 |
| O3 | 4*e* | 0.701(6) | 0.210(6) | 0.022(6) | 1.0000 | 2.0000 |
| $x = 0.5$ ($P2_1/n$) | | | | | | |
| Sr | 4*e* | 0.482(2) | 0.0117(8) | 0.253(4) | 0.76(11) | 2.0000 |
| Ni1/Mn1/Te1 | 2*a* | 0.0000 | 0.0000 | 0.0000 | 0.1(4) | 0.366(4)/0.434(4)/0.20(4) |
| Ni2/Mn2/Te2 | 2*b* | 0.0000 | 0.0000 | 0.5000 | 0.9(3) | 0.134(4)/0.066(4)/0.800(4) |
| O1 | 4*e* | 1.067(8) | 0.003(6) | 0.742(4) | 1.07(2) | 2.0000 |
| O2 | 4*e* | 0.261(12) | 0.270(14) | 0.999(10) | 1.07(2) | 2.0000 |
| O3 | 4*e* | 0.802(10) | 0.288(12) | −0.027(14) | 1.07(2) | 2.0000 |
| $x = 0.75$ ($I2/m$) | | | | | | |
| Sr | 4*i* | 0.496(3) | 0.0000 | 0.7631(7) | 1.44(10) | 2.0000 |
| Ni1/Mn1/Te1 | 2*d* | 0.5000 | 0.5000 | 0.0000 | 0.17682 | 0.610(5)/0.200(5)/0.190(5) |
| Ni2/Mn2/Te2 | 2*a* | 0.0000 | 0.0000 | 0.0000 | 2.68(17) | 0.140 (5)/0.055(5)/0.81(5) |
| O1 | 4*i* | −0.095(5) | 0.0000 | 0.767(6) | 1.00000 | 2.0000 |
| O2 | 8*j* | 0.255(5) | 0.259(5) | 0.984(9) | 1.00000 | 4.0000 |

according to Glazer notation. Identically understanding from Figure 5(b) about the connection between the octahedras $(Mn/Ni/Te)_{2d}O_6$ and $(Mn/Ni/Te)_{2a}O_6$ defined by the $I2/m$ model and Figure 5(d) provides the tilt system ($a^-a^-c^0$) as suggested by Glazer for this monoclinic centered system.

A structural analysis of the monoclinic compositions of this series was carried out suggests that the sites of the ($Ni^{2+}/Mn^{2+}$) and $Te^{6+}$ cations are coordinated by six oxygens in a distorted octahedral arrangement. The oxygen atoms (for $x = 0.25$ and 0.5) connect the $(Mn/Ni/Te)_{2a}O_6$ and $(Mn/Ni/Te)_{2b}O_6$ octahedra along the three directions. The same fact for the composition ($x = 0.75$), we have observed that the octahedra $(Mn/Ni/Te)_{2d}O_6$ and $(Mn/Ni/Te)_{2a}O_6$ are bound by the oxygen atoms in the three directions. The bond distance values (see Table IV) are in good agreement with those found in related double perovskite compounds (Ortega-San Martin *et al*., 2004; Ortega-San Martin *et al*., 2005a, 2005b).

Note that many reports show that if the charge of *B* and *B*' are different in the ordered double perovskite structure, the oxygen ions are slightly displaced to the more charged cation despite the fact that the octahedral symmetry of the $BO_6$ and $B'O_6$ units is preserved. This determination is in agreement with the fact that $Te^{6+}$ is more charged than ($Mn^{2+}/Ni^{2+}$), making a bigger distance between ($Mn^{2+}/Ni^{2+}$) and oxygen, unlike the $Te^{6+}$ having a smaller distance with oxygen (see Table IV). We also noticed the values of the lengths and the angles of connection between the cations and the oxygens reveal some distortions of the octahedra [$(Mn/NiTe)_{2a}O_6$ and $(Mn/Ni/Te)_{2b}O_6$] for ($x = 0.25$ and 0.5), and the octahedra [$(Mn/NiTe)_{2d}O_6$ and $(Mn/Ni/Te)_{2a}O_6$] for ($x = 0.75$).

The liaison of the octahedra $(Mn/Ni/Te)_{2a}O_6$ and $(Mn/Ni/Te)_{2b}O_6$-octahedra for the two compositions ($x = 0.25$ and 0.5) of the series $Sr_2Mn_{1-x}Ni_xTeO_6$ is made by the oxygen O(1) atoms along the *c*-axis, and in the *ab*-plane the connection is made by the two oxygen atoms O(2) and O(3). The tilt of the octahedral is seen from the three bond angles $(Mn/Ni/Te)_{2a}$–O(1)–$(Mn/Ni/Te)_{2b}$ (171.4°), $(Mn/Ni/Te)_{2a}$–O(2)–$(Mn/Ni/Te)_{2b}$ (153.0°), and $(Mn/Ni/Te)_{2a}$–O(3)–$(Mn/Ni/Te)_{2b}$ (167°). Concerning the composition ($x = 0.75$), the connection of the octahedra $(Mn/Ni/Te)_{2d}O_6$ and $(Mn/Ni/Te)_{2a}O_6$-octahedra is performed by the oxygen O(1) atoms along the *c*-axis, and in the *ab*-plane the linking is made by the O (2) atoms. The incline of the octahedral is noticed from the two bond angles $(Mn/Ni/Te)_{2d}$–O(1)–$(Mn/Ni/Te)_{2a}$ (155°) and $(Mn/Ni/Te)_{2d}$–O(2)–$(Mn/Ni/Te)_{2a}$ (171.1°) (see Table IV).

The Sr atoms form polyhedral ($SrO_{12}$) with Sr–O bond lengths between 2.3 and 3.3 Å and an average value d of about 2.8 Å. For the two compositions ($x = 0.25$ and 0.5) with $P2_1/n$ space group, the sharing faces of $SrO_{12}$ polyhedral are connected by oxygen O(2) and O(3) along the axis *c*, in the *ab*-plane these polyhedral are connected by four oxygen atoms O(1) [see Figure 5(e)].

About the composition ($x = 0.75$) crystallizing in $I2/m$ space group, the connection of the face of the polyhedral $SrO_{12}$ is made by oxygen O(1) along the axis *c*, while in the *ab*-plane they are linked by four oxygen atoms O(2). We reveal the arrangement of atoms in the $SrO_{12}$ polyhedron sites in Figure 5(f).

### C. The Raman and IR spectroscopy studies

In this section of the paper Raman and IR spectroscopy studies were undertaken, to obtain further structural information about the nature of bonding in this series of double perovskite $Sr_2Mn_{1-x}Ni_xTeO_6$ with ($x = 0.25$, 0.5, and 0.75). We have utilized group theory to classify the vibratory states of our double perovskite series.

The analysis of the site symmetry group (see Table V) of the compounds $Sr_2Mn_{1-x}Ni_xTeO_6$ ($x = 0.25$, 0.5, and 0.75) of the double perovskite structure [with $P2_1/n$ and $I2/m$ space group, ($C2/m$ point group)] led to the following irreducible representation (Kroumova *et al*., 2003).

$T\ (P2_1/n) = 3A_g\ (R) + 3B_g\ (R) + 12A_u\ (IR) + 12B_u\ (IR) + A_u\ (ac)\ 2B_u\ (ac)$


https://doi.org/10.1017/S0885715619000411 Published online by Cambridge University Press

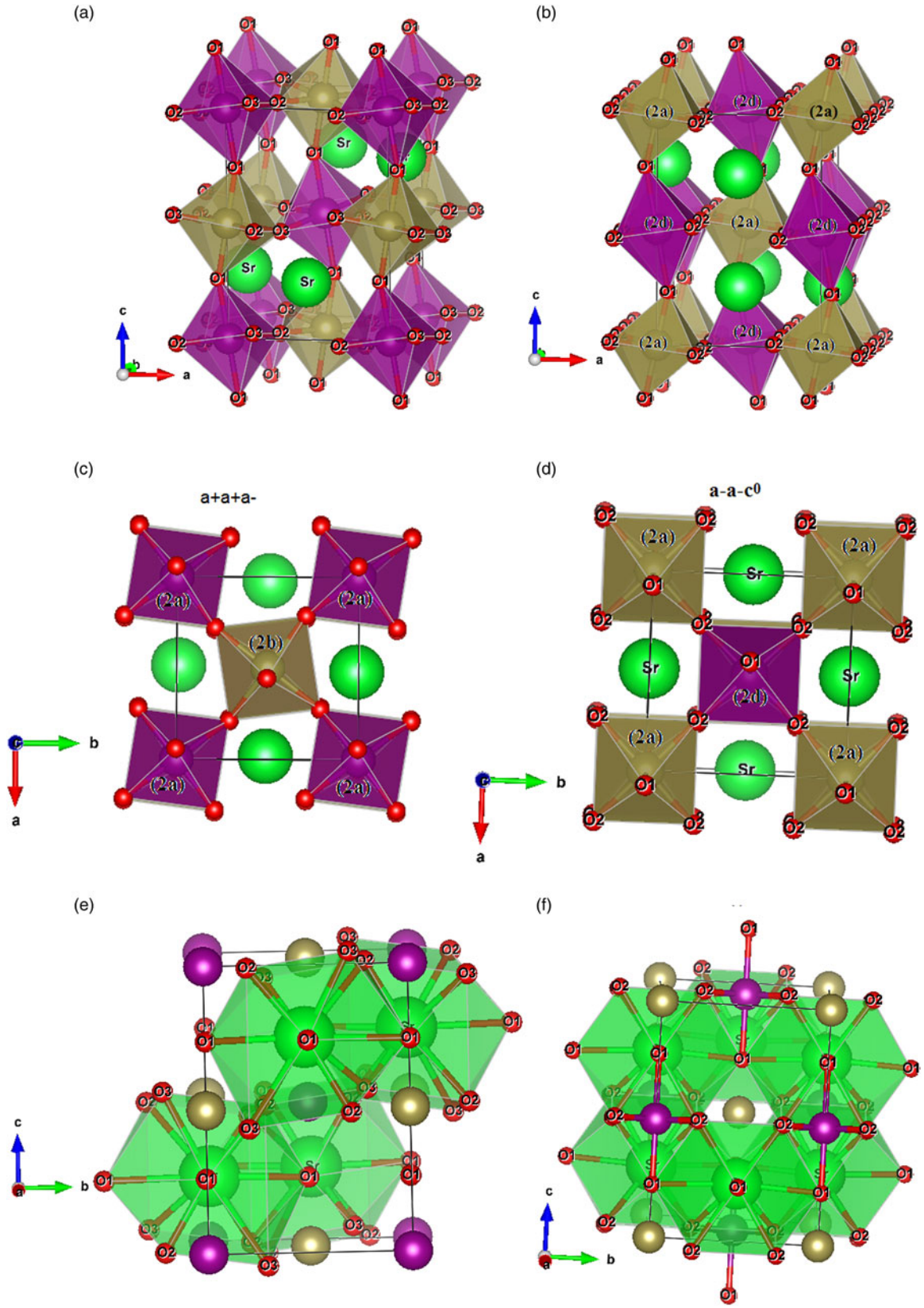


Figure 5. (Colour online) Crystal structures of a double perovskite series $Sr_2Mn_{1-x}Ni_xTeO_6$ with ($x = 0.25$, 0.5 and 0.75) generated by VESTA program. (a) and (b) show the alternation and tilting of the octahedral for the compositions $Sr_2Mn_{0.5}Ni_{0.5}TeO_6$ and $Sr_2Mn_{0.25}Ni_{0.75}TeO_6$ crystallizing in space groups $P2_1/n$ and $I2/m$, respectively. (c) and (d) indicate the structure in-phase (+) and out-of-phase (−) rotations of the compositions in $P2_1/n$ and $I2/m$, respectively. (e) and (f) show the polyhedral $(Sr)O_{12}$ setting in $P2_1/n$ and $I2/m$ symmetries.


https://doi.org/10.1017/S0885715619000411 Published online by Cambridge University Press

TABLE IV. The inter – atomic distances (Å) and angles (°) selected at room temperature for the monoclinic compositions in $Sr_2Mn_{1-x}Ni_xTeO_6$ ($x = 0.25$, 0.5, and 0.75) series.

| Compositions | $x = 0.25$ | $x = 0.5$ | $x = 0.75$ | |
|---|---|---|---|---|
| Octahedra site: (2*a*) | | | | |
| Mn1/Ni1/Te1–O1 | 2.06(2) | 2.09(6) | 2.19(6) | |
| Mn1/Ni1/Te1–O2 | 2.06(6) | 2.12(6) | 1.94(3) | |
| Mn1/Ni1/Te–O3 | 2.07(6) | 1.98(6) | – | |
| Average distance | 2.06(6) | 2.07 | 2.07 | |
| Predicted distance | 2.00 | 2.02 | 2.04 | |
| Octahedra site: (2*b*) | | | | |
| Mn2/Ni2/Te2–O1 | 1.97(2) | 1.96(6) | 1.93(6) | |
| Mn2/Ni2/Te2–O2 | 1.93(5) | 1.87(6) | 1.99(3) | |
| Mn2/Ni2/Te2–O3 | 1.99(5) | 2.08(6) | – | |
| Average distance | 1.97 | 1.96 | 1.96 | |
| Predicted distance | 1.95 | 1.94 | 1.92 | |
| Internal angles/° | | | | |
| O1–Mn1/Ni1/Te1–O2 | 91(3) | 104(5) | 103(4) | |
| O1–Mn1/Ni1/Te1–O3 | 95(3) | 102(5) | – | |
| O2–Mn1/Ni1/Te1–O3 | 105(5) | 93(4) | – | |
| O2–Mn1/Ni1/Te1–O2 | – | – | 94(2) | |
| Internal angles/° | | | | |
| O1–Mn2/Ni2/Te2–O2 | 94(3) | 101(5) | 102(4) | |
| O1–Mn2/Ni2/Te2–O3 | 92(3) | 101(5) | – | |
| O2–Mn2/Ni2/Te2–O3 | 104(3) | 90(4) | – | |
| O2–Mn2/Ni2/Te2–O2 | – | – | 93(2) | |
| External angles/° | | | | |
| Mn1/Ni1–O1–Te2 | 171.4(10) | 160(2) | 155(2) | |
| Mn1/Ni1–O2–Te2 | 153(2) | 163(2) | 171.1(13) | |
| Mn1/Ni1–O3–Te2 | 167(2) | 139(3) | – | |
| SrO12 icosahedron | | | SrO12 icosahedron | |
| Sr–O1 | 3.26(2) | 3.10(5) | Sr–O1 | 3.18(6) |
| Sr–O1 | 2.41(2) | 2.55(5) | Sr–O1 | 2.46(6) |
| Sr–O1 | 2.84(3) | 2.93(3) | Sr–O1 × 2 | 2.850(8) |
| Sr–O1 | 2.94(3) | 2.78(3) | Sr–O2 × 2 | 2.66(4) |
| Sr–O2 | 3.23(3) | 2.60(6) | Sr–O2 × 2 | 2.98(4) |
| Sr–O2 | 2.61(3) | 2.84(6) | Sr–O2 × 2 | 2.97(4) |
| Sr–O2 | 3.19(3) | 2.85(6) | Sr–O2 × 2 | 2.65(4) |
| Sr–O2 | 2.36(3) | 2.98(5) | Average distance | 2.8 |
| Sr–O3 | 2.89(4) | 3.30(6) | Predicted distance | 2.9 |
| Sr–O3 | 2.83(4) | 2.85(6) | | |
| Sr–O3 | 2.85(4) | 2.91(6) | | |
| Sr–O3 | 2.71(4) | 2.28(6) | | |
| Average distance | 2.60 | 2.8 | | |
| Predicted distance | 2.9 | 2.9 | | |

$T\ (I2/m) = 7A_g\ (R) + 5B_g\ (R) + 7A_u\ (IR) + 11B_u\ (IR) + A_u$ (ac) $2B_u$ (ac)

The symbols stand for: R – Raman active modes, IR – IF active modes, ac – acoustic modes.

### 1. Raman spectroscopy

In Figure 6 we present the Raman spectra of the series $Sr_2Mn_{1-x}Ni_xTeO_6$ with ($x = 0.25$, 0.5, and 0.75) recorded at room temperature CCD to avoid stitching artifacts, a laser type DPSS (Spectra-Physics, 600 nm, 8 mW). The Raman result is in good agreement with the literature of these double perovskite compounds that crystallize in a monoclinic symmetry.

When we have analyzed the factor group, we have found that six active modes of Raman, represented by $\lambda$ (Raman) = $3A_g + 3B_g$, ought to be observed for monoclinic compositions with a space group of $P2_1/n$, and twelve active modes of Raman [$\lambda$ (Raman) = $7A_g(R) + 5B_g$ (R)] should be observed for monoclinic compositions with a space group *I*2/*m*. From the analysis of the spectra, it has been found that most of the bands of our system are weak; there are only three bands and they are observed around (~412, ~550, and ~750 $cm^{-1}$). The modes observed and the assignment, are recorded in Table VI.

According to several studies already done on this type of material (Manoun *et al*., 2012; Tamraoui *et al*., 2014), we can classify the Raman modes observed in our double perovskite series $Sr_2Mn_{1-x}Ni_xTeO_6$ ($x = 0.25$, 0.5, and 0.75) into three general families of network vibrations:

– At wavenumbers under <350 $cm^{-1}$, there are translations of the cations $Sr^{2+}$, also translational and rotational modes of the *B*'$O_6$ octahedral.
– The region 350−500 $cm^{-1}$, concerns the bending vibrations of O–(*B*')–O.
– At wavenumbers above 550 $cm^{-1}$, there are stretching modes of (*B*')–O.


https://doi.org/10.1017/S0885715619000411 Published online by Cambridge University Press

TABLE V. Factor group analysis of the series $Sr_2Mn_{1-x}Ni_xTeO_6$ with ($x = 0.25$, 0.5, and 0.75) at room temperature (Kroumova *et al.*, 2003).

| symmetry | Atom | Site | $A_g$ | $A_u$ | $B_g$ | $B_u$ | Modes |
|---|---|---|---|---|---|---|---|
| $P2_1/n$ | Te | 2*b* | | 6 | | 6 | $M = 6A_u + 6B_u$ |
| | Mn, Ni | 2*a* | | 6 | | 6 | $M = 6A_u + 6B_u$ |
| | Sr | 4*e* | 3 | 6 | 3 | 6 | $M = 3A_g + 6A_u + 3B_g + 6B_u$ |
| | O1 | 4*e* | 3 | 6 | 3 | 6 | $M = 3A_g + 6A_u + 3B_g + 6B_u$ |
| | O2 | 4*e* | 3 | 6 | 3 | 6 | $M = 3A_g + 6A_u + 3B_g + 6B_u$ |
| | O3 | 4*e* | 3 | 6 | 3 | 6 | $M = 3A_g + 6A_u + 3B_g + 6B_u$ |
| | $T_{total} = 48A + 48B = 96$ $T_{acustic} = A_u + 2B_u$ | | | | | | |
| | $T_{Raman} = 12A_g + 12B_g$ $T_{infrared} = 36A_u + 36B_u$ | | | | | | |
| *I*2/*m* | Te | 2*a* | | 1 | | 2 | $M = 1A_u + 2B_u$ |
| | Mn, Ni | 2*d* | | 1 | | 2 | $M = 1A_u + 2B_u$ |
| | Sr | 4*i* | 2 | 1 | 1 | 2 | $M = 2A_g + A_u + B_g + 2B_u$ |
| | O1 | 4*i* | 2 | 1 | 1 | 2 | $M = 2A_g + A_u + B_g + 2B_u$ |
| | O2 | 8*j* | 3 | 3 | 3 | 3 | $M = 3A_g + 3A_u + 3B_g + 3B_u$ |
| | $T_{total} = 14A + 16B = 30$ $T_{acustic} = A_u + 2B_u$ | | | | | | |
| | $T_{Raman} = 7A_g + 5B_g$ $T_{infrared} = 7A_u + 11B_u$ | | | | | | |

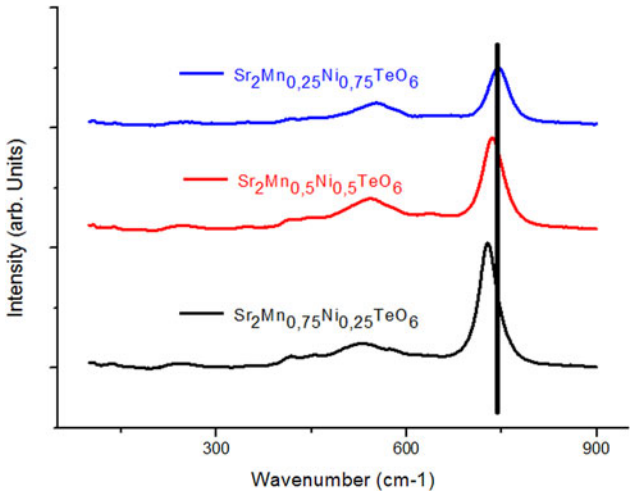


Figure 6. (Colour online) Raman spectra of the series $Sr_2Mn_{1-x}Ni_xTeO_6$ with ($x = 0.25$, 0.5, and 0.75) recorded at ambient conditions. The vertical lines on the bands of the Raman spectra to signal the small change in the modes produced into this series of double perovskite.

The investigation of Raman spectra recorded at room temperature of these double perovskite compounds $Sr_2Mn_{1-x}Ni_xTeO_6$ with ($x = 0.25$, 0.5 and 0.75) demonstrates that there are astounding changes in Raman modes in the arrangement of the series, this changing is between $Sr_2Mn_{0.5}Ni_{0.5}TeO_6$ and $Sr_2Mn_{0.25}Ni_{0.75}TeO_6$.

It was discovered that, other than its effect on the cell parameters, the concentration of the Ni and Mn cations likewise impacts the [(Mn/Ni)–O and Te–O] distances. We observed that the frequency of the $\upsilon_1$ mode increments straightly with expanding of the Nickel concentration in this series of double pérovskite. To clarify these results, we considered that the frequency of the $\upsilon_1$ is corresponding to the Te–O bonding energies. Table IV shows that the Te–O distances in connection to the apical and equatorial oxygens diminish. This effect expands the Te–O bonding energy, therefore we had an expanding of the $\upsilon_1$ mode frequency (Ayala *et al.*, 2007).

### 2. Infrared spectroscopy

In Figure 7 we give the IF spectra, for the arrangement of the $Sr_2Mn_{1-x}Ni_xTeO_6$ mixes prepared. The most striking component obvious from this figure is the enormous closeness between the compounds in the IF spectra mostly for the two compounds $Sr_2Mn_{0.75}Ni_{0.25}TeO_6$ and $Sr_2Mn_{0.5}Ni_{0.5}TeO_6$, while the IF spectra of the compound $Sr_2Mn_{0.25}Ni_{0.75}TeO_6$ are different from the others, especially at the level of the band situated around the recurrence 750 $cm^{-1}$.

Accordingly, the point that can be promptly deduced from the vibrational spectra that the degree of cation order into each composition gives off an impression of the whole arrangement of mixes. The sharp bands present in these spectra are demonstrative of an arranged dissemination of Te.

## IV. CONCLUSION

In this work we have presented the synthesis, the analyzed by conventional XRPD, the refinements using the Rietveld method. The structural analysis shows that ($Mn^{2+}$ and $Ni^{2+}$) and $Te^{6+}$ are divided between the *B* and *B*' sites of the double

TABLE VI. Raman and infrared shift (in $cm^{-1}$) for the observed modes in $Sr_2Mn_{0.75}Ni_{0.25}TeO_6$, $Sr_2Mn_{0.5}Ni_{0.5}TeO_6$, and $Sr_2Mn_{0.25}Ni_{0.75}TeO_6$.

| $\upsilon$ ($Sr_2Mn_{0.75}Ni_{0.25}TeO_6$) | $\upsilon$ ($Sr_2Mn_{0.50}Ni_{0.50}TeO_6$) | $\upsilon$ ($Sr_2Mn_{0.25}Ni_{0.75}TeO_6$) | Assignment |
|---|---|---|---|
| Raman | | | |
| 136 | very weak | very weak | T |
| 410 | 411 | 413 | $\upsilon_5$ |
| 550 | 551 | 553 | $\upsilon_2$ |
| 748 | 749 | 752 | $\upsilon_1$ |
| Infrared | | | |
| 695 | 699 | 710 | $\upsilon_1$ |


https://doi.org/10.1017/S0885715619000411 Published online by Cambridge University Press

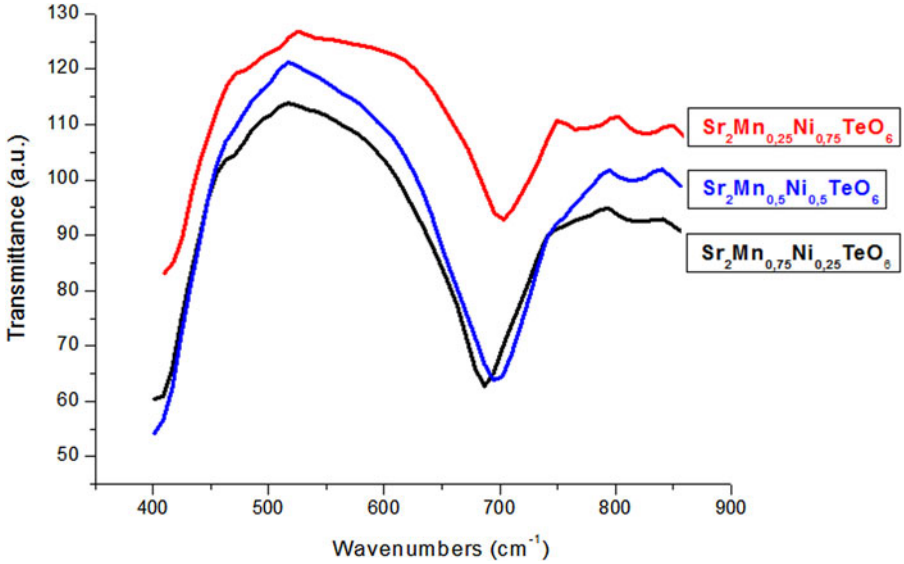


Figure 7. (Colour online) The infrared spectra of $Sr_2Mn_{1-x}Ni_xTeO_6$ ($x = 0.25$, 0.5, and 0.75) compounds. The vertical lines on the bands show the little change in the modes produced into this series of double perovskite.

perovskite structure $A_2BB'TeO_6$. We have introduced and confirmed by Raman and IR spectroscopy the phase transition producing the change in the double perovskite structure (from $P2_1/n$ to $I2/m$) with the increase of the nickel composition in the series $Sr_2Mn_{1-x}Ni_xTeO_6$. Even though we observed from the Raman and IR spectra a small number of vibratory mode numbers, in contrast to those given by the group theory, all the spectra show the regular band pattern characteristic of the double perovskite structure. The vibrational modes were examined as far as the oxygen octahedra inward vibrations demonstrating that the fundamental unit in the structures of these materials is the $TeO_6$. This exhibit gives a reason for the lessened number of groups seen in the Raman spectra and gives a helpful technique in describing the phase transitions as far as the gathering subgroup symmetry connection of these vibrational modes.

## SUPPLEMENTARY MATERIAL

The supplementary material for this article can be found at https://doi.org/10.1017/S0885715619000411

## ACKNOWLEDGEMENTS

The authors would like to acknowledge University Hassan II, Casablanca, Morocco, for their support. The authors are grateful to Engineers [in Service Centrale d'Analyse (CSA) de l'Unités d'Appui Technique à la Recherche Scientifique (UATRS) CNRS – Rabat, Morocco] for technical assistance.

Ayala, A. P., Guedes, I., Silva, E. N., Augsburger, M. S., del C. Viola, M., and Pedregosa, J. C. (**2007**). "Raman investigation of $A_2CoBO_6$ (A = Sr and Ca, B = Te and W) double perovskites," J. Appl. Phys. **101**, 123511.

Azad, A.K., Eriksson, S.-G., Rundlöf, H., and Eriksen, J. (**2004**). "Synthesis and crystal structure of the double perovskite $Ca_{2-x}Sr_xMnWO_6$ (x = 0.0, 0.5, 1.0, 1.5, 2.0)," Mater. Sci. Forum. **443–444**, 375–378.

Bernardo, P. L., Ghivelder, L., Eslava, G. G., Amorim, H. S., Felner, I., and Garcia, S. (**2014**). "Monoclinic distortion and magnetic coupling in the double perovskite $Sr_{2-x}Ca_xYRuO_6$," J. Solid State Chem. **220**, 270–276.

Cecilia Blanco, M., De Paoli, J. M., Ceppi, S., Tirao, G., Nassif, V. M., Guimpel, J., and Carbonio, R. E. (**2014**). "Synthesis, structural characterization and magnetic properties of the monoclinic ordered double perovskites $BaLaMSbO_6$, with M = Mn, Co and Ni," J. Alloys Compd. **606**, 139–148.

Gandhi, A., and Keshri, S. (**2015**). "Microwave dielectric properties of double perovskite ceramics Ba2Zn1-xCaxWO6 ($x = 0$–0.4)," Ceram. Int. **41**, 3693–3700.

Ghimire, M. P., Kaphle, G. C., and Thapa, R. K. (**2016**). "Electronic and magnetic properties of double perovskites $Nd_2MgIrO_6$," J Nepal Phys. Soc. **3**, 50.

Glazer, A. M. (**1975**). "Simple ways of determining perovskite structures," Acta Crystallogr. **A31**, 756.

Halder, A., Nafday, D., Sanyal, P., and Saha-Dasgupta, T. (**2018**). "Computer predictions on Rh-based double perovskites with unusual electronic and magnetic properties," npj. Qautum Materials **3**, 17.

Knapp, M. C., and Woodward, P. M. (**2006**). "A-site cation ordering in $AA'BB'O_6$ perovskites," J. Solid State Chem. **179**, 1076–1085.

Kroumova, E., Aroyo, M. I., Perez-Mato, J. M., Kirov, A., Capillas, C., Ivantchev, S.; Wondratschek, H. (**2003**). "Bilbao Crystallographic Server: useful databases and tools for phase-transition studies," Phase Transit. **76**, 155. http://www.cryst.ehu.es /.

Li, Z., Cho, Y., Li, X., Li, X., Aimi, A., Inaguma, Y., Antonio Alonso, J., Teresa Fernandez-Diaz, M., Yan, J., Downer, M. C., Henkelman, G., Goodenough, J. B., and Zhou, J. (**2018**). "New mechanism for ferroelectricity in the perovskite $Ca_{2-x}Mn_xTi_2O_6$ synthesized by spark plasma sintering," J. Am. Chem. Soc. **140**, 2214–2220.

Manoun, B., Ezzahi, A., Benmokhtar, S., Ider, A., Lazor, P., Bih, L., and Igartua, J. M. (**2012**). "X-ray diffraction and Raman spectroscopy studies of temperature and composition induced phase transitions in $Ba_{2-x}Sr_xZnWO_6$ ($0 \leq x \leq 2$) double perovskite oxides," J. AlloysCompd. **533**, 43–52.

Mugavero, S. J., Puzdrjakova, I. V., Smith, M. D., and zur Loye, H. C. (**2005**). "$Sm_2nairo_6$, a monoclinically distorted double perovskite," Acta Crystallogr. **E61**, i3–i5.

Musa Saad, H.-E. M. (**2014**). "DFT-FPLMTO study of electronic and magnetic structures of half-metallic antiferromagnetic complex perovskite Ba2CoWO6," Comput. Condens. Matter. **1**, 14–18.

Ochi, M., Yamada, I., Ohgushi, K., Kusano, Y., Mizumaki, M., Takahashi, R., Yagi, S., Nishiyama, N., Inoue, T., and Irifune, T. (**2013**). "B-site deficiencies in A-site-ordered perovskite $LaCu_3Pt_{3.75}O_{12}$," Inorg. Chem. **52**, 3985–3989.

Orayech, B., Ortega-San-Martín, L., Urcelay-Olabarria, I., Lezama, L., Rojo, T., Arriortua, M. I., and Igartuag, J. M. (**2015**). "Structural phase transitions and magnetic and spectroscopic properties of the double perovskites $Sr_2Co_{1-x}Mg_xTeO_6$ ($x = 0.1$, 0.2 and 0.5)," Dalton Trans. **44**, 13716.

Ortega-San Martin, L., Chapman, J. P., Hernandez Bocanegra, E., Insausti, M., Arriortua, M. I., and Rojo, T. (**2004**). "Structural phase transitions in the ordered double perovskite $Sr_2MnTeO_6$," J. Phys.: Condens. Matter. **16**, 3879–3888.

Ortega-San Martin, L., Chapman, J. P., Cuello, G., Gonzalez-Calbet, J., Arriortua, M. I., and Rojo, T. (**2005a**). "Crystal structure of the ordered double perovskite, $Sr_2NiTeO_6$," Z. Anorg. Allg. Chem. **631**, 2127–2130.

Ortega-San Martin, L., Chapman, J. P., Lezama, L., Sanchez-Marcos, J., Rodriguez-Fernandez, J., Isabel Arriortuab, M., and Rojo, T. (**2005b**). "Factors determining the effect of Co(II) in the ordered double perovskite structure: sr2CoTeO6," J. Mater. Chem. **15**, 183–193.

Pena, M. A., and Fierro, J. L. G. (**2001**). "Chemical structures and performance of perovskite oxides," Chem. Rev. **101**, 1981–2017.

Prior, T. J., Couper, V. J., and Battle, P. D. (**2005**). "Structural chemistry of the cation-ordered perovskites $Sr_2CaMo_{1-x}Te_xO_6$ ($0 \leq x \leq 1$)," J. Solid State Chem. **178**, 153–157.

Rodriguez-Carvajal, J. (**1997**). "Fullprof, Program for Rietveld refinement," Laboratoire Léon Brillouin (CEA-CNRS), Saclay, France.

Roisnel, T., and Rodriguez-Carvajal, J. (**2001**). "WinPLOTR: a Windows tool for powder diffraction pattern analysis," Mater. Sci. Forum. **378–381**, 118–123.

Shannon, R. D. (**1976**). "Revised effective ionic radii and systematic studies of interatomie distances in halides and chaleogenides," Acta Crystallogr. **A32**, 75.

Tamraoui, Y., Manoun, B., Mirinioui, F., Haloui, R., and Lazor, P. (**2014**). "X-ray diffraction and Raman spectroscopy studies of temperature and composition induced phase transitions in $Ba_{2-x}Sr_xMgTeO_6$ ($0 \leq x \leq 2$)," J. Alloys Compd. **603**, 86–94.

Tang, Y., Hunter, E. C., Battle, P. D., Sena, R. P., Hadermann, J., Avdeev, M., and Cadogan, J. M. (**2016**). "Structural chemistry and magnetic properties of the perovskite $Sr_3Fe_2TeO_9$," J. Solid State Chem. **242**, 86–95.

Tang, Y., Sena, R. P., Avdeev, M., Battle, P. D., Cadogan, J. M., Hadermann, J., and Hunter, E. C. (**2017**). "Magnetic properties of the 6H perovskite $Ba_3Fe_2TeO_9$," J. Solid State Chem. **253**, 347–354.

Tasca, J. E., Lavata, A. E., and Gloria González, M. (**2017**). "Double perovskites $La_2MMnO_6$ as catalyst for propane combustion," J. Asian Ceram. Soc. **5**, 235–241.

Venevtsev, Y. N., Politova, E. D., and Zhdanov, G. S. (**1974**). "Tellurium containing ferroelectrics: X-ray data, dielectric properties, phase transitions," Ferroelectrics **8**, 489–490.

Zamkova, N. G., Zhandun, V. S., and Zinenko, V. I. (**2013**). "First principles calculations of ferroelectric properties in AA'BB'$O_6$ double perovskites with different types of cation ordering," Phys. Status Solidi B., 1–10.

Zaraq, A., Orayech, B., Faik, A., Igartua, J. M., Jouanneaux, A., and El Bouari, A. (**2016**). "High temperature induced phase transitions in $SrCaCoTeO_6$ and $SrCaNiTeO_6$ ordered double perovskites," Polyhedron **110**, 119–124.



https://doi.org/10.1017/S0885715619000411 Published online by Cambridge University Press